AIMS Mathematics, 11(5): 13589–13616.
DOI: 10.3934/math.2026559
Received: 01 March 2026
Revised: 20 April 2026
Accepted: 29 April 2026
Published: 15 May 2026

http://www.aimspress.com/journal/Math

Research article

Adaptive and fractional-order super-twisting (FO-STA) control for trajectory tracking of mobile robots with differential traction

Sahbi Boubaker[1,*], Jorge Uliarte[2], Flavio Capraro[3], Souad Kamel[1], Faisal S. Alsubaei[4], Farid Bourennani[5] and Francisco Rossomando[3]

[1] Department of Computer and Network Engineering, College of Computer Science and Engineering, University of Jeddah, Jeddah 21959, Saudi Arabia
[2] Facultad de Ingenieria, Universidad Nacional de Cuyo (UNCu), Centro Universitario, M5502JMA, Mendoza, Argentina
[3] Instituto de Automatica, UNSJ-CONICET, San Juan, CP 5400, Argentina
[4] Department of Cybersecurity, College of Computer Science and Engineering, University of Jeddah, Jeddah 23218, Saudi Arabia
[5] Department of Information Systems and Technology, College of Computer Science and Engineering, University of Jeddah, Jeddah 23218, Saudi Arabia

* **Correspondence:** Email: sboubaker@uj.edu.sa.

Abstract: Differential-drive mobile robots (DDMRs) are extensively used in logistics applications such as warehouse automation, last-mile delivery, and material handling owing to their simple mechanical structure and high maneuverability. Nevertheless, achieving accurate trajectory tracking remains challenging due to nonholonomic constraints, parameter uncertainties, wheel slip, and external disturbances in dynamic environments. Motivated by the inherent symmetry in the kinematic and dynamic structure of DDMRs, this paper proposes an adaptive control and a fractional-order super-twisting Algorithm (FO-STA)-based control framework for robust trajectory tracking using a dynamic model. The proposed approach adopted a dual-loop control architecture composed of an external kinematic loop and an inner dynamic loop, forming a robust control structure. The kinematic controller ensures convergence of the robot position to the desired reference trajectory, while the dynamic controller compensates for model uncertainties and external disturbances to achieve stable velocity tracking. An adaptive FO-STA mechanism was incorporated to enhance robustness against time-varying dynamics and unknown parameter variations. Both control laws were systematically derived using Lyapunov stability theory, guaranteeing closed-loop convergence and boundedness of tracking errors. Simulation results confirmed the effectiveness of the proposed strategy, demonstrating accurate trajectory tracking and strong robustness under parameter uncertainties and external disturbances, thereby validating its suitability for logistics-oriented mobile robotic systems.

Keywords: differential drive mobile robot; stability analysis; trajectory tracking; fractional-order control; super-twisting algorithm; logistics
Mathematics Subject Classification: 93-10, 93D21

1. Introduction

Mobile robots with differential traction have emerged as one of the most efficient and versatile platforms for modern logistics and last-mile delivery applications, both in indoor and outdoor environments. Their mobility principle, based on independently driven wheels, offers high maneuverability, enabling tight turns, zero-radius rotation, and smooth navigation in narrow, dynamic spaces such as warehouses, malls, hospitals, and university campuses. This mechanical simplicity translates into reduced hardware complexity, easier maintenance, and lower energy consumption compared to omnidirectional or multi-wheel robotic configurations. However, these same characteristics generate complex dynamic behaviors, derived from uncontrolled lateral slippage and the non-uniform distribution of contact forces between the vehicle and the ground. Consequently, the accurate modeling and control of mobile robots (in their various configurations) remain an active challenge in control research, see [1–5]. Due to the vehicle's dynamics, in Nezhad et al. [6], a strategy for wheeled vehicles, in which the dynamics of self-balancing two-wheeled mobile robots were decomposed into fully actuated and underactuated subsystems, was presented. For the former, a fast terminal sliding-mode controller was designed. For the latter, a sliding-mode control strategy that integrates two fast terminal sliding surfaces was used. Leader-follower control for heterogeneous wheeled mobile robots was developed, which employed multiple control strategies, in which each robot's control is implemented using an improved sliding-mode control (SMC) strategy with fuzzy logic control developed at the tracking layer [7]. But traditionally, trajectory tracking in mobile robots (DDMR, SSMR (Skid Steering Mobile Robot), and others) has been addressed using idealized kinematic models that assume simple geometric relationships between wheel speeds and body movement [8, 9]. These models allow for the synthesis of lightweight controllers, but fail to capture critical effects such as wheel-ground interaction, coupling between longitudinal and lateral speeds, torque saturation, and the nonlinearity inherent in slippage. Such omissions negatively impact tracking accuracy and can compromise system stability, especially at high speeds or during aggressive maneuvers [10, 11]. In response to these limitations, in recent years, there has been growing interest in control strategies based on complete dynamic models, capable of representing more realistically the distribution of forces, inertial effects, and the contribution of drive torques in generating motion. Such models allow the coupled behavior of velocities to be captured and improve the controller's ability to compensate for disturbances and unmodeled dynamics. However, the explicit incorporation of dynamics introduces new challenges: the presence of uncertain parameters (such as soil-dependent friction coefficients), high nonlinearity, and the need for advanced, robust, or adaptive control techniques [12]. While system uncertainties and external disturbances are the main causes of degraded trajectory tracking performance in nonholonomic wheeled mobile robots (NWMRs), [13] proposed a fast non-singular terminal sliding mode adaptive dynamic control method (AFNTSMDC) to provide robust and improved finite-time tracking performance for differential-type nonholonomic

mobile robots. The proposed controller has a simple form and does not have singularity problems at the control input, making it easy to implement. The stability of the control law was demonstrated using the Lyapunov function. Finally, the AFNTSMDC scheme was compared with existing methods in the presence of uncertainties and external disturbances. In another proposal by Cao [14], he offered a second-order terminal sliding mode (2TSM) approach to track the trajectory of the differential drive mobile robot (DDMR). Within this cascade control scheme, the 2TSM dynamic controller in the inner control loop tracks the DDMR's velocities, while the outer loop (kinematic controller) adjusts the robot's positions. This guaranties convergence in finite time thanks to the second-order TSM manifold, which involves higher-order derivatives of the state variables, resulting in good, robust, and fast tracking accuracy. The results obtained in simulation demonstrate the authors' claims. [15] proposed a fixed-time consensus control algorithm for nonlinear stochastic multiagent systems (SNMASs) with non-triangular structure and input saturation using the command-filtered backstepping design method. Fuzzy logic systems were used to identify the nonlinear dynamics of each agent. The paper presented a comparative simulation example applying the proposed fixed-time consensus control strategy. Similarly, [16] addressed the problem of adaptive sliding mode trajectory tracking control for mobile wheeled robots in the presence of external disturbances and inertia uncertainties. A new fast nonsingular terminal sliding mode surface without any constraints was proposed, preserving the advantages of sliding mode control and avoiding singularity issues. First, a fast nonsingular adaptive terminal sliding mode control law for angular velocity was constructed to stabilize the second-order subsystem in finite time. Next, another fast nonsingular adaptive terminal sliding mode control law for linear velocity was designed to ensure the stability of the third-order subsystem. The validity of the scheme is demonstrated with a simulation example. Other techniques using SMC was presented by [17], which designed a time delay estimation (TDE) scheme for unknown nonlinear robotic systems with uncertainty and external disturbances that uses fractional-order fixed-time sliding mode control (TDEFxFSMC). The FxSMC method allows high-performance tracking positions to be obtained, immune to vibrations with fixed-time non-singular control. The paper showed the results of the technique applied to the nonlinear dynamics of robots with unknown dynamics in trajectory tracking. In contrast, [18] presented a control method based on fast terminal sliding mode inverse dynamics PID (Proportional-Integral-Derivative) for wheeled mobile robots (WMRs). Due to nonlinear and nonholonomic properties, under the assumption that it is difficult to establish an adequate model of the mobile robot system for trajectory tracking, the authors implemented a PID control based on fast terminal sliding mode control to ensure asymptotic stabilization of the robot's position and orientation around the desired trajectory, taking into account the robot's kinematics and dynamics. The authors presented simulation work demonstrating robust trajectory tracking of mobile robots. One of the proposals to address this type of problem was presented by [19], in which the authors presented the design and implementation of a modified super-twisting algorithm (STA) controller that functions as a step-by-step differentiator and estimates the speed and acceleration of the mobile robot. Next, a second STA imposes the tracking of a predefined trajectory. The numerical and experimental results comparing the STA with a state feedback controller (SFC) and a first-order sliding mode controller (FOSM) justifed the control proposal. Also, [20] implemented a super-torsional sliding mode adaptive controller. An uncertain drift term was assumed to be bounded by an unknown limit. The proposed Lyapunov-based approach consisted of using control gains adapted from the STA algorithm to ensure convergence in finite time

to a second-order sliding mode. Viability was demonstrated with a numerical example. In this context, this paper developed a trajectory control strategy for DDMR robots based on reduced dynamics but considering dynamic uncertainties in the model, with the aim of improving tracking accuracy and robustness against terrain variations and operating conditions. The proposed approach integrates STA and adaptive controller (AC) where the proposed controller reduces errors due to uncertainties. The adaptive controller adjusts the parameters to reduce dynamic uncertainties, and the STA technique eliminates residual uncertainty. Simulation results demonstrate that the method achieves significantly superior performance to purely kinematic controllers, especially in highly demanding maneuvers. The main contributions of this work can be summarized as follows:

- Design of a fractional-order STA and adaptive control for DDMRs to mitigate or reduce uncertainties and disturbances by acting on its dynamics.
- Application of a multivariable FO-STA-AC technique in dynamical systems.
- Two nested loops and kinematic control for an FO-STA-AC control system, in which the kinematic controller provides the speed references.
- Stability analysis of the nested loop system (kinematic controller-FO-STA-AC) demonstrating the overall stability of the control proposal.

The remaining sections of this paper are organized as follows: Section 2 presents the mathematical representation of the complete DDMR model. Section 3 illustrates the design of the kinematics model. The FO-STA-AC controller is discussed in Section 4. The corresponding stability analysis is depicted in Section 5. Section 6 presents the results of simulated scenarios under various conditions, which allow perceiving the good performance of the proposed adaptive controller. Finally, conclusions are given in Section 8.

2. Differential drive mobile robot model

In this section, the kinematic model of the DDMR is presented. In order to develop the kinematic model of the DDMR, a velocity constraint must be introduced: $v + a_0\omega = 0, z = 0$ presented by [10]. This restriction represents the nonholonomic constraint that bounds the x-position of the instantaneous center of rotation (ICR) in the DDMR base, avoiding severe loss of stability due to elevated skidding.

$$\underbrace{\begin{pmatrix}\dot{x}\\ \dot{y}\\ \dot{\Psi}\end{pmatrix}}_{\dot{\bar{\mathbf{x}}}} = \underbrace{\begin{pmatrix}\cos\Psi(t) & -a_0\sin\Psi(t)\\ \sin\Psi(t) & a_0\cos\Psi(t)\\ 0 & 1\end{pmatrix}}_{\mathbf{R}^*(\Psi(t))}\underbrace{\begin{pmatrix}v\\ \omega\end{pmatrix}}_{\mathbf{v}} \tag{2.1}$$

and, in compact form, this can be represented as:

$$\dot{\bar{\mathbf{x}}} = \mathbf{R}^*(\Psi(t))\mathbf{v}. \tag{2.2}$$

We have $\mathbf{v} = \left(v, \omega\right)^T \in \mathbb{R}^{2\times 1}$ and $\bar{\mathbf{x}} = \left(x, y, \Psi\right)^T \in \mathbb{R}^{3\times 1}$.

The kinematic model can be represented by:

$$\underbrace{\begin{pmatrix}\dot{x}\\ \dot{y}\end{pmatrix}}_{\dot{\mathbf{x}}} = \underbrace{\begin{pmatrix}\cos\Psi(t) & -a_0\sin\Psi(t)\\ \sin\Psi(t) & a_0\cos\Psi(t)\end{pmatrix}}_{\mathbf{R}(\Psi(t))}\underbrace{\begin{pmatrix}v\\ \omega\end{pmatrix}}_{\mathbf{v}}. \tag{2.3}$$

This last equation will be used to develop the kinematic controller in the next section (3).

It should be noted that the dynamics of a DDMR present an inherent symmetry in their control actions due to their mechanical design. The two independently driven wheels are mounted on a common axle, with the origin of the reference frame normally located at the midpoint between the wheels. For this reason, torque-based control actions are symmetric for each wheel (taking into account the torque = 0 axis). Another feature to consider is that the center of mass is located on the axis of symmetry (the longitudinal axis is perpendicular to the wheel axis), shown in Figure 1. Future work will focus on kinematic control with posture control (taking into account the orientation Ψ). The dynamic model of the DDMR of mass m and moment of inertia J_z was analyzed in [21] and evaluated the dimensional sensitivity of maximum traction and braking force, considering chassis forces. The model was designed for an agricultural environment. This model can be used to predict 2-D movement on a planar surface:

$$\begin{pmatrix}\dot{v}\\ \dot{\omega}\end{pmatrix} = -\begin{pmatrix}\frac{c_r v}{m+\frac{2I_w}{r^2}}\\ \frac{c_\omega\omega}{J_z+\frac{2I_w L^2}{2r^2}}\end{pmatrix} + \begin{pmatrix}\frac{1}{(rm+\frac{2I_w}{r})} & \frac{1}{(rm+\frac{2I_w}{r})}\\ -\frac{d}{(J_z+\frac{2I_w d^2}{r})} & \frac{d}{(J_z+\frac{2I_w d^2}{r})}\end{pmatrix}\begin{pmatrix}\tau_L\\ \tau_R\end{pmatrix} + \begin{pmatrix}\delta_L\\ \delta_R\end{pmatrix}, \tag{2.4}$$

where:

r is the distance from the center of the drive shaft to the point of contact with the ground,

c_r, c_ω are friction coefficients,

δ_L, δ_R are model uncertainties,

τ_L and τ_R are the torque on the left and right wheels respectively,

m is the mass of DDMR,

J_z is the moment of inertia around the z-axis,

I_w is the moment of inertia of each wheel z-axis,

L is the width of the robot measured between the geometric center of the wheels/tracks on the left side and the right side.

x, y are the coordinates of the DDMR in the XY plane,

x_{ref}, y_{ref} are desired coordinate points of the DDMR in the XY plane,

v and ω are the linear and angular velocities developed by the DDMR, respectively.

G indicates the DDMR's center of mass.

$\mathbf{x}$ is the point where the vehicle is referenced containing the coordinates x, y.

Ψ indicates the orientation of the robot.

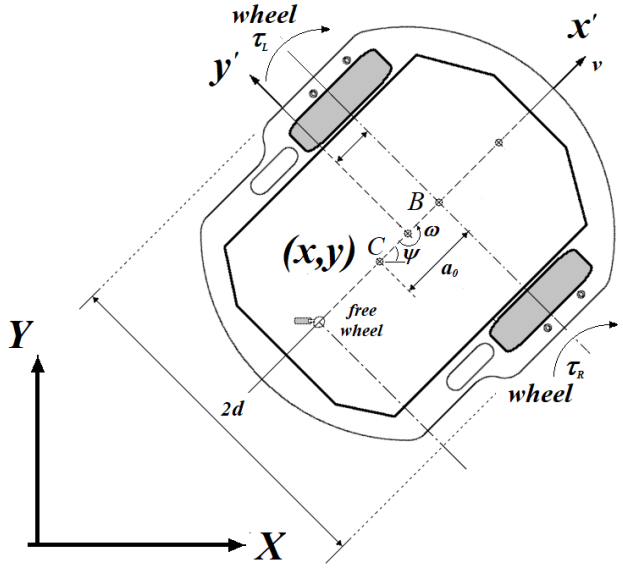

Figure 1. DDMR parameters.

The values of the parameters are shown in Table 2 in the Appendix A.
We can represent Eq (2.4) in compact form as:

$$\dot{\mathbf{v}} = \mathbf{K}_A\mathbf{v} + \mathbf{K}_B\mathbf{u} + \mathbf{\Delta}, \tag{2.5}$$

where:

$$\mathbf{K}_A = \begin{pmatrix} \frac{c_r}{m+\frac{2I_w}{r^2}} & 0 \\ 0 & \frac{c_\omega}{J_z+\frac{2I_wL^2}{2r^2}} \end{pmatrix}, \quad \mathbf{K}_B = \begin{pmatrix} \frac{1}{(rm+\frac{2I_w}{r})} & \frac{1}{(rm+\frac{2I_w}{r})} \\ -\frac{d}{(J_z+\frac{2I_wd^2}{r})} & \frac{d}{(J_z+\frac{2I_wd^2}{r})} \end{pmatrix}, \quad \mathbf{\Delta} = \begin{pmatrix} \delta_L \\ \delta_R \end{pmatrix},$$

and the state vector and the input vector are defined as:

$$\mathbf{v} = \begin{pmatrix} \dot{v} \\ \dot{\omega} \end{pmatrix} \quad \mathbf{u} = \begin{pmatrix} \tau_L \\ \tau_R \end{pmatrix}. \tag{2.6}$$

For the application of an effective control technique that allows for the adjustment of dynamic variations, two control loops will be used: an external loop to adjust the position of the robot, and an internal loop to compensate for possible dynamic variations. These will be discussed in Sections (3) and (4), respectively.

3. External loop control design

This control proposal employs a nestled control scheme consisting of two controllers: a kinematic controller and a dynamic controller (Figure 2). The kinematic control is based on inverse kinematics and relies on the kinematic model of the DDMR described in (2.3). First, it is necessary to define the position error as:

$$\tilde{\mathbf{x}} = \mathbf{x}_{\text{ref}} - \mathbf{x} = \begin{pmatrix} \tilde{x} \\ \tilde{y} \end{pmatrix} = \begin{pmatrix} x_{\text{ref}} \\ y_{\text{ref}} \end{pmatrix} - \begin{pmatrix} x \\ y \end{pmatrix}. \tag{3.1}$$

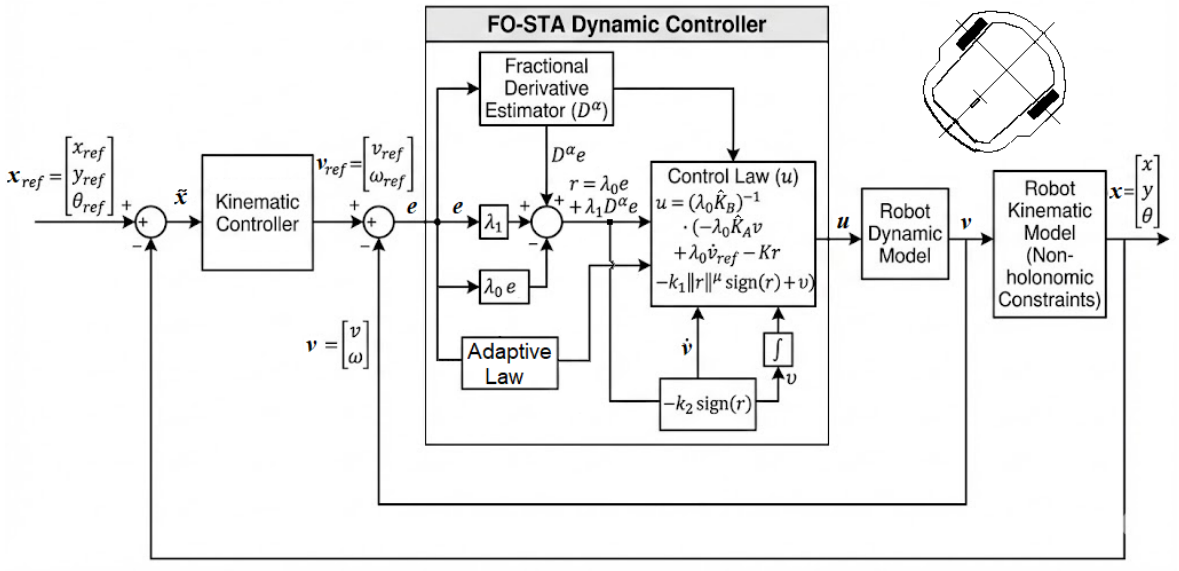

Figure 2. Block diagram of the proposed two-level control approach.

The kinematic control law is shown below.

$$\mathbf{v}_{\text{ref}} = \begin{pmatrix} v_{\text{ref}} \\ \omega_{\text{ref}} \end{pmatrix} = \underbrace{\begin{pmatrix} \cos(\Psi) & \sin(\Psi) \\ -\dfrac{1}{a_0}\sin(\Psi) & \dfrac{1}{a_0}\cos(\Psi) \end{pmatrix}}_{\mathbf{R}(\Psi)^{-1}} \underbrace{\begin{pmatrix} \dot{x}_{\text{ref}} - k_x\tilde{x} \\ \dot{y}_{\text{ref}} - k_y\tilde{y} \end{pmatrix}}_{\left(\dot{\mathbf{x}}_{ref} - \mathbf{K}_p\tilde{\mathbf{x}}\right)}, \tag{3.2}$$

where:

- $\dot{x}_{\text{ref}}, \dot{y}_{\text{ref}}$: derivatives of the reference positions along the x and y axes.
- $\mathbf{r}$: reference velocities vector,
- $\tilde{x}, \tilde{y}$: trajectory tracking errors along the x and y axes,
- $\mathbf{K}_p$: matrix of control gains for the kinematic controller $\mathbf{K}_p = \text{diag}(k_x, k_y)$.

Replacing (3.2) in (2.3) (assuming perfect velocity tracking), and then $\mathbf{v} = \mathbf{v}_{ref}$, the external closed-loop equation results in:

$$\begin{pmatrix} \dot{x} \\ \dot{y} \end{pmatrix} = \underbrace{\begin{pmatrix} \cos(\Psi) & -a_0\sin(\Psi) \\ \sin(\Psi) & a_0\cos(\Psi) \end{pmatrix}}_{\mathbf{R}(\Psi)} \underbrace{\begin{pmatrix} \cos(\Psi) & \sin(\Psi) \\ -\dfrac{1}{a_0}\sin(\Psi) & \dfrac{1}{a_0}\cos(\Psi) \end{pmatrix}}_{\mathbf{R}(\Psi)^{-1}} \underbrace{\begin{pmatrix} \dot{x}_{\text{ref}} - k_x\tilde{x} \\ \dot{y}_{\text{ref}} - k_y\tilde{y} \end{pmatrix}}_{\left(\dot{\mathbf{x}}_{ref} - \mathbf{K}_p\tilde{\mathbf{x}}\right)} \tag{3.3}$$

with:

$$\begin{pmatrix} \dot{x} \\ \dot{y} \end{pmatrix} = \begin{pmatrix} \dot{x}_{\text{ref}} \\ \dot{y}_{\text{ref}} \end{pmatrix} - \begin{pmatrix} k_x\tilde{x} \\ k_y\tilde{y} \end{pmatrix} \tag{3.4}$$

or

$$\underbrace{\begin{pmatrix}\dot{\tilde{x}}\\ \dot{\tilde{y}}\end{pmatrix}}_{\dot{\tilde{\mathbf{x}}}} = \underbrace{-\begin{pmatrix}k_x\tilde{x}\\ k_y\tilde{y}\end{pmatrix}}_{\left(\mathbf{K}_p\tilde{\mathbf{x}}\right)}. \tag{3.5}$$

Now, we select a candidate Lyapunov function of the form:

$$\mathcal{L}_K = \frac{1}{2}\tilde{\mathbf{x}}^T\tilde{\mathbf{x}}. \tag{3.6}$$

Deriving (3.6) and replacing (3.5) leads to:

$$\dot{\mathcal{L}}_K = \tilde{\mathbf{x}}^T\dot{\tilde{\mathbf{x}}} = -\tilde{\mathbf{x}}^T\mathbf{K}_p\tilde{\mathbf{x}} < 0. \tag{3.7}$$

With this result, it is easy to see that $\tilde{\mathbf{x}} \to 0$ when $t \to \infty$. In the following section, the assumption of perfect speed tracking is abandoned, considering dynamic variations.

4. Inner loop control

In this section, a fractional-order controller [22] is proposed. In general, conventional controllers that use instantaneous errors to define control action do not respond well to persistent disturbances, such as viscous friction. One way to solve this problem is to apply fractional calculus theory (FCT) [23, 24] by incorporating a fractional order into the super-twisting sliding surface architecture, including a "memory" function controller to take into account historical control error information. The fractional-order basic operator $\mathcal{D}_t^\alpha$ can be defined as given below:

$$\mathcal{D}_t^\alpha = \begin{cases} \frac{d^\alpha}{dt^\alpha}, & \alpha > 0, \\ 1, & \alpha = 0, \\ \int_t^0 (d\tau)^\alpha, & \alpha < 0. \end{cases} \tag{4.1}$$

This method can be adjusted based on its design, as the dynamics of the control system are scalable, allowing for optimization of the balance between speed and damping. The great advantage of these FO-STA techniques is that they use weighted integration of past errors, formulated based on Caputo's definition [25, 26], allowing the controller to adapt to variations in dynamics (e.g., displacement of the vehicle's center of mass, persistent friction, etc.). Using Caputo's definition, the fractional-order operator can be represented by:

$$\mathcal{D}_t^\alpha e(t) = \frac{1}{\Gamma(n-\alpha)}\int_0^t \frac{e^{(n)}(\tau)}{(t-\tau)^{\alpha-n+1}}d\tau. \tag{4.2}$$

From the above equation, the derivative α of the control error signal $e(t)$is $m < 1$, where $m \in N$ and Γ are the gamma functions, whereas the Caputo differential derivative operator can be represented by $\mathcal{D}^\alpha$. The proposed control structure is shown in Figure 2 illustrates the FO control system, and the analysis is based on the mathematical model of DDMR dynamics in (2.5).

Consideration 1: It is assumed that $\mathbf{\Delta}(t)$ is a bounded function.

$$\|\boldsymbol{\Delta}(t)\| < \delta_0, \quad \forall t > 0. \tag{4.3}$$

Consideration 2: The velocity vector reference, $\mathbf{v}_{ref}$, is assumed to be at least twice differentiable. Furthermore,

$$\mathbf{v}_{ref}, \dot{\mathbf{v}}_{ref}, \ddot{\mathbf{v}}_{ref} < \kappa_0, \quad \forall t > 0. \tag{4.4}$$

$\mathbf{v}_{ref}$ must satisfy smoothness, differentiability, and boundedness conditions to ensure stability and accurate tracking.

Therefore, the control errors are defined as follows:

$$\mathbf{e} = \mathbf{v} - \mathbf{v}_{ref}. \tag{4.5}$$

Consider the control errors and define the fractional sliding surface as:

$$\mathbf{r} = \mathbf{e} + \lambda_1 \mathcal{D}^{\alpha} \mathbf{e}, \tag{4.6}$$

where $\lambda_1 > 0$ and $0 < \alpha < 1$. Then the time derivative of (4.6) leads to:

$$\dot{\mathbf{r}} = \dot{\mathbf{e}} + \lambda_1 \frac{d}{dt}(\mathcal{D}^{\alpha} \mathbf{e}) = \dot{\mathbf{e}} + \lambda_1 \mathcal{D}^{\alpha+1} \mathbf{e}. \tag{4.7}$$

Next, we replace (4.5) and (4.6) in (4.7),

$$\dot{\mathbf{r}} = (\dot{\mathbf{v}} - \dot{\mathbf{v}}_{ref}) + \lambda_1 \mathcal{D}^{\alpha+1} \mathbf{e} = \left(\mathbf{K}_A \mathbf{v} + \mathbf{K}_B \mathbf{u} + \boldsymbol{\Delta} - \dot{\mathbf{v}}_{ref}\right) + \lambda_1 \mathcal{D}^{\alpha+1} \mathbf{e}. \tag{4.8}$$

Therefore, $\dot{\mathbf{r}}$ can be obtained from (4.8) and results in

$$\dot{\mathbf{r}} = \mathbf{K}_A \mathbf{v} + \mathbf{K}_B \mathbf{u} + \boldsymbol{\Delta} - \dot{\mathbf{v}}_{ref} + \lambda_1 \mathcal{D}^{\alpha+1} \mathbf{e} = \mathbf{K}_A \mathbf{v} + \mathbf{K}_B \mathbf{u} - \dot{\mathbf{v}}_{ref} + \boldsymbol{\phi}(t), \tag{4.9}$$

where $\boldsymbol{\phi}(t) = \boldsymbol{\Delta} + \lambda_1 \mathcal{D}^{\alpha+1} \mathbf{e}$ represents a total perturbation term. According to Consideration 2, it follows that $\boldsymbol{\phi}(t)$ is bounded by a positive constant ϕ_0, such that $\|\boldsymbol{\phi}(t)\| \leq \phi_0$. On the other hand, the matrices $\mathbf{K}_B$ and $\mathbf{K}_A$ represent the dynamic of the DDMR, some of which are unknown and may vary during the trajectory tracking. Therefore, it is necessary to work with estimates of the dynamics. Which we denoted as $\hat{\mathbf{K}}_B$ and $\hat{\mathbf{K}}_A$. Based on (4.9), the proposed controller for a DDMR is:

$$\mathbf{u} = (\hat{\mathbf{K}}_B)^{-1}\Big(- \hat{\mathbf{K}}_A \mathbf{v} + \dot{\mathbf{v}}_{ref} - \mathbf{K}\mathbf{r}\Big). \tag{4.10}$$

Basically, this proposal is a combination of the STA technique, the adaptive controller (AC), and fractional calculation, which maintains the robustness and simplicity of the STA controller. The FO-STA-AC proposal differs from the integer-order STA controller presented in the works [19, 27–29]. Furthermore, in this proposal, the FO-STA is a modification of the traditional STA controller in order to obtain a better response. On the other hand, the FO-STA is presented by:

$$\begin{cases} \mathbf{u}_{sw} = -k_1 (\|\mathbf{r}\|)^{\mu} \dfrac{\mathbf{r}}{\|\mathbf{r}\|} + \boldsymbol{\upsilon}, \\ \dot{\boldsymbol{\upsilon}} = -k_2 \dfrac{\mathbf{r}}{\|\mathbf{r}\|}. \end{cases} \tag{4.11}$$

In the above Eq (4.11), k_1, k_2 and μ are the design parameters (k_1,$k_2 > 0$ and $0 < \mu < 1$) that the designer should take into account. This equation defines the sliding mode component ($\mathbf{u}_{sv}$) of the control law, which incorporates the fractional sliding surface ($\mathbf{r}$), the design parameters (k_1, k_2, μ), and an auxiliary variable ($\boldsymbol{\nu}$) to achieve finite-time convergence of the tracking error. Therefore, Eq (4.10), taking into account (4.11) ($\mathbf{u} + \mathbf{u}_{sw}$), will be expressed as:

$$\begin{cases} \mathbf{u} = (\hat{\mathbf{K}}_B)^{-1}\Big(- \hat{\mathbf{K}}_A\mathbf{v} + \dot{\mathbf{v}}_{ref} - \mathbf{K}\mathbf{r} - k_1(\|\mathbf{r}\|)^{\mu}\dfrac{\mathbf{r}}{\|\mathbf{r}\|} + \boldsymbol{\upsilon}\Big), \\ \dot{\boldsymbol{\upsilon}} = -k_2\dfrac{\mathbf{r}}{\|\mathbf{r}\|}. \end{cases} \tag{4.12}$$

The previous equation provides the complete control law ($\mathbf{u}$) applied to the DDMR dynamics. It combines the estimates of the robot's dynamics ($\hat{\mathbf{K}}_A, \hat{\mathbf{K}}_B$) with the reference acceleration ($\dot{\mathbf{v}}_{ref}$), the term ($-\mathbf{K}\mathbf{r}$), and the robust fractional super-twisting term. To close the control loop, it is necessary to operate in (4.9) by adding and subtracting $\hat{\mathbf{K}}_B\mathbf{u}$.

$$\dot{\mathbf{r}} = \mathbf{K}_A\mathbf{v} + \mathbf{K}_B\mathbf{u} + \hat{\mathbf{K}}_B\mathbf{u} - \hat{\mathbf{K}}_B\mathbf{u} + \boldsymbol{\phi}(t) - \dot{\mathbf{v}}_{ref}. \tag{4.13}$$

In addition, replacing Eq (4.12) in (4.13), the closed control loop is,

$$\begin{cases} \dot{\mathbf{r}} = -\mathbf{K}\mathbf{r} - k_1(\|\mathbf{r}\|)^{\mu}\dfrac{\mathbf{r}}{\|\mathbf{r}\|} + \boldsymbol{\upsilon} + \Big(\underbrace{\mathbf{K}_A - \hat{\mathbf{K}}_A}_{\tilde{\mathbf{K}}_A}\Big)\mathbf{v} + \Big(\underbrace{\mathbf{K}_B - \hat{\mathbf{K}}_B}_{\tilde{\mathbf{K}}_B}\Big)\mathbf{u} + \boldsymbol{\phi}(t), \\ \dot{\boldsymbol{\upsilon}} = -k_2\dfrac{\mathbf{r}}{\|\mathbf{r}\|}. \end{cases} \tag{4.14}$$

Recalling $\tilde{\mathbf{K}}_A = \mathbf{K}_A - \hat{\mathbf{K}}_A$ and $\tilde{\mathbf{K}}_B = \mathbf{K}_B - \hat{\mathbf{K}}_B$, and replacing in (4.14),

$$\begin{cases} \dot{\mathbf{r}} = -\mathbf{K}\mathbf{r} - k_1(\|\mathbf{r}\|)^{\mu}\dfrac{\mathbf{r}}{\|\mathbf{r}\|} + \boldsymbol{\upsilon} - \tilde{\mathbf{K}}_A\mathbf{v} + \tilde{\mathbf{K}}_B\mathbf{u} + \boldsymbol{\phi}(t), \\ \dot{\boldsymbol{\upsilon}} = -k_2\dfrac{\mathbf{r}}{\|\mathbf{r}\|}. \end{cases} \tag{4.15}$$

In the Eq (4.15), the term $\boldsymbol{\phi}(t)$ represents the whole perturbation and undesired elements. In the next Section this term will be reduced with the FO-STA-AC term. Furthermore, this fractional surface is conditioned by the parametric errors of the model. It is important to note at this point that the main contribution of this work is the application of the FO-STA-AC technique to multivariable dynamic systems. In our specific case, this involves the development of FO-STA-AC control for DDMR-type mobile robots. The following section includes a stability analysis of the proposed technique, for which we will analyze these conditions ensuring the system stability.

5. Stability analysis and tuning rules

In this section, the stability of the control system (FO-STA-AC) will be analyzed and the conditions for online estimation of the DDMR parameters will be obtained, which will be used in the proposed controller.

Theorem 1. The dynamic of the control system, defined in (4.15), presents an asymptotic stability using the control law given in (4.12).

Proof. We propose the Lyapunov function (positive definite) as:

$$\mathcal{L}(\mathbf{r}, \boldsymbol{\nu}, \tilde{\mathbf{K}}_A, \tilde{\mathbf{K}}_B) = k_2\|\mathbf{r}\| + \frac{1}{2}\boldsymbol{\nu}^T\boldsymbol{\nu} + \frac{1}{2b_A}tr(\tilde{\mathbf{K}}_A\tilde{\mathbf{K}}_A^T) + \frac{1}{2b_B}tr(\tilde{\mathbf{K}}_B\tilde{\mathbf{K}}_B^T). \tag{5.1}$$

Parameters b_A and b_B are constant and $0 < b_A, b_B < 1$. By deriving Eq (5.1), we obtain

$$\dot{\mathcal{L}}(\mathbf{r}, \boldsymbol{\nu}, \tilde{\mathbf{K}}_A, \tilde{\mathbf{K}}_B) = k_2\frac{d\|\mathbf{r}\|}{dt} + \boldsymbol{\nu}^T\dot{\boldsymbol{\nu}} + \frac{1}{b_A}tr(\tilde{\mathbf{K}}_A\dot{\tilde{\mathbf{K}}}_A^T) + \frac{1}{b_B}tr(\tilde{\mathbf{K}}_B\dot{\tilde{\mathbf{K}}}_B^T). \tag{5.2}$$

Considering the chain rule for $\dfrac{d\|\mathbf{r}\|}{dt} = \dfrac{\partial\|\mathbf{r}\|}{\partial\mathbf{r}}\dfrac{\partial\mathbf{r}}{\partial t} = \dfrac{\mathbf{r}^T}{\|\mathbf{r}\|}\dot{\mathbf{r}}$ leads to:

$$\dot{\mathcal{L}}(\mathbf{r}, \boldsymbol{\nu}, \tilde{\mathbf{K}}_A, \tilde{\mathbf{K}}_B) = k_2\frac{\mathbf{r}^T}{\|\mathbf{r}\|}\dot{\mathbf{r}} + \boldsymbol{\upsilon}^T\dot{\boldsymbol{\upsilon}} + \frac{1}{b_A}tr(\tilde{\mathbf{K}}_A\dot{\tilde{\mathbf{K}}}_A^T) + \frac{1}{b_B}tr(\tilde{\mathbf{K}}_B\dot{\tilde{\mathbf{K}}}_B^T). \tag{5.3}$$

Then, Eq (4.15) is replaced in (5.3),

$$\begin{aligned}\dot{\mathcal{L}}(\mathbf{r}, \boldsymbol{\nu}, \tilde{\mathbf{K}}_A, \tilde{\mathbf{K}}_B) &= k_2\frac{\mathbf{r}^T}{\|\mathbf{r}\|}\Big(-\mathbf{K}\mathbf{r} - (\|\mathbf{r}\|)^\mu k_1\frac{\mathbf{r}}{\|\mathbf{r}\|} + \boldsymbol{\upsilon} - \tilde{\mathbf{K}}_A\mathbf{v} + \tilde{\mathbf{K}}_B\mathbf{u} + \boldsymbol{\phi}(t)\Big) + ... \\ &+ \boldsymbol{\upsilon}^T\Big(-k_2\frac{\mathbf{r}}{\|\mathbf{r}\|}\Big) + \frac{1}{b_A}tr\Big(\tilde{\mathbf{K}}_A\dot{\tilde{\mathbf{K}}}_A^T\Big) + \frac{1}{b_B}tr\Big(\tilde{\mathbf{K}}_B\dot{\tilde{\mathbf{K}}}_B^T\Big).\end{aligned} \tag{5.4}$$

Applying the distributive property,

$$\begin{aligned}\dot{\mathcal{L}}(\mathbf{r}, \boldsymbol{\nu}, \tilde{\mathbf{K}}_A, \tilde{\mathbf{K}}_B) &= -\Big(k_2\frac{\mathbf{r}^T}{\|\mathbf{r}\|}\mathbf{K}\mathbf{r} - k_1k_2(\|\mathbf{r}\|)^\mu + k_2\frac{\mathbf{r}^T}{\|\mathbf{r}\|}\boldsymbol{\upsilon} - k_2\frac{\mathbf{r}^T}{\|\mathbf{r}\|}\tilde{\mathbf{K}}_A\mathbf{v} + \\ &+ k_2\frac{\mathbf{r}^T}{\|\mathbf{r}\|}\tilde{\mathbf{K}}_B\mathbf{u} + k_2\frac{\mathbf{r}^T}{\|\mathbf{r}\|}\boldsymbol{\phi}(t)\Big) - k_2\boldsymbol{\upsilon}^T\frac{\mathbf{r}}{\|\mathbf{r}\|} + \\ &+ \frac{1}{b_A}tr\Big(\tilde{\mathbf{K}}_A\dot{\tilde{\mathbf{K}}}_A^T\Big) + \frac{1}{b_B}tr\Big(\tilde{\mathbf{K}}_B\dot{\tilde{\mathbf{K}}}_B^T\Big).\end{aligned} \tag{5.5}$$

Given the scalar equivalence $k_2\frac{\mathbf{r}^T}{\|\mathbf{r}\|}\boldsymbol{\upsilon} = k_2\boldsymbol{\upsilon}^T\frac{\mathbf{r}}{\|\mathbf{r}\|}$, and utilizing the cyclic property of the trace in Eq (5.5), it follows that:

$$\begin{cases}\dfrac{\mathbf{r}^T}{\|\mathbf{r}\|}\tilde{\mathbf{K}}_A\mathbf{v} = tr\Big(\dfrac{\mathbf{r}^T}{\|\mathbf{r}\|}\tilde{\mathbf{K}}_A\mathbf{v}\Big) = tr\Big(\tilde{\mathbf{K}}_A\mathbf{v}\dfrac{\mathbf{r}^T}{\|\mathbf{r}\|}\Big), \\ \dfrac{\mathbf{r}^T}{\|\mathbf{r}\|}\tilde{\mathbf{K}}_B\mathbf{u} = tr\Big(\dfrac{\mathbf{r}^T}{\|\mathbf{r}\|}\tilde{\mathbf{K}}_B\mathbf{u}\Big) = tr\Big(\tilde{\mathbf{K}}_B\mathbf{u}\dfrac{\mathbf{r}^T}{\|\mathbf{r}\|}\Big)\end{cases} \tag{5.6}$$

and replacing (5.6) in (5.5), we have:

$$\begin{aligned}\dot{\mathcal{L}} &= -k_2\frac{\mathbf{r}^T}{||\mathbf{r}||}\mathbf{K}\mathbf{r} - k_1k_2(||\mathbf{r}||)^\mu + k_2\frac{\mathbf{r}^T}{||\mathbf{r}||}\boldsymbol{\phi}(t) + ... \\ &+ tr\left(\tilde{\mathbf{K}}_B\left[k_2\mathbf{u}\frac{\mathbf{r}^T}{||\mathbf{r}||} + \frac{1}{b_B}\dot{\tilde{\mathbf{K}}}_B^T\right]\right) + ... \\ &+ tr\left(\tilde{\mathbf{K}}_A\left[-k_2\mathbf{v}\frac{\mathbf{r}^T}{||\mathbf{r}||} + \frac{1}{b_A}\dot{\tilde{\mathbf{K}}}_A^T\right]\right). \end{aligned} \tag{5.7}$$

In the above Eq (5.7), taking into account the terms in parentheses, it is possible to define the adjustment rules for $\dot{\tilde{\mathbf{K}}}_A$ and $\dot{\tilde{\mathbf{K}}}_B$ as:

$$\begin{cases} \dot{\tilde{\mathbf{K}}}_B = -b_Bk_2\dfrac{\mathbf{r}}{||\mathbf{r}||}\mathbf{u}^T, \\ \dot{\tilde{\mathbf{K}}}_A = b_Ak_2\dfrac{\mathbf{r}}{||\mathbf{r}||}(\mathbf{v})^T. \end{cases} \tag{5.8}$$

If the matrices of constant parameters $\mathbf{K}_A$ and $\mathbf{K}_B$ are considered over a period of time ($\frac{d\mathbf{K}_A}{dt} = 0$ and $\frac{d\mathbf{K}_B}{dt} = 0$), the expressions for $\dot{\tilde{\mathbf{K}}}_A$ and $\dot{\tilde{\mathbf{K}}}_B$ can be represented as

$$\begin{cases} \dot{\tilde{\mathbf{K}}}_B = -b_Bk_2\dfrac{\mathbf{r}}{||\mathbf{r}||}\mathbf{u}^T, \\ \dot{\tilde{\mathbf{K}}}_A = b_Ak_2\dfrac{\mathbf{r}}{||\mathbf{r}||}(\mathbf{v})^T. \end{cases} \tag{5.9}$$

Equations (5.9) are tuning rules of the adaptive part of the proposed controller (FO-STA-AC). Now, replacing these equations in (5.7), the $\dot{\mathcal{L}}$ can be represented as:

$$\dot{\mathcal{L}} = -k_2\frac{\mathbf{r}^T}{||\mathbf{r}||}\mathbf{K}|\mathbf{r}| - k_1k_2(||\mathbf{r}||)^\mu + k_2\frac{\mathbf{r}^T}{||\mathbf{r}||}\boldsymbol{\phi}(t). \tag{5.10}$$

By Considerations 1 and 2, the function $\boldsymbol{\phi}$ is bounded, therefore, $||\boldsymbol{\phi}|| \leq \phi_o$. In Eq (5.10), if $k_1(||\mathbf{r}||)^\mu \geq ||\boldsymbol{\phi}||$, then $\dot{\mathcal{L}} \leq 0$. This condition leads to $k_1 \geq \frac{\phi_o}{(||\mathbf{r}||)^\mu}$ and the stability is guaranteed. The state variables $\mathbf{r}$, $\boldsymbol{\nu}$, $\tilde{\mathbf{K}}_A$, and $\tilde{\mathbf{K}}_B$ are bounded. Now, applying the integral defined in the interval $[0, t_f]$ over Eq (5.10), we obtain:

$$\int_0^{t_f}\Big(k_2\frac{\mathbf{r}^T}{||\mathbf{r}||}\mathbf{K}|\mathbf{r}|\Big)dt \leq \int_0^{t_f}\frac{d}{dt}\Big(-\mathcal{L}(t)\Big)dt = \mathcal{L}(0) - \mathcal{L}(t_f). \tag{5.11}$$

$\mathcal{L}(t_f) > 0$ because $\mathcal{L}$ is a positive definite function. Disregarding this last term, the above equation can be rewritten as:

$$\mathcal{L}(0) \geq \int_0^{t_f} k_2\frac{\mathbf{r}^T}{||\mathbf{r}||}\mathbf{K}|\mathbf{r}|dt. \tag{5.12}$$

Here, $\mathbf{K}$ denotes a positive definite matrix whose minimum and maximum eigenvalues are $\lambda_{\min}$ and $\lambda_{\max}$, respectively. Therefore,

$$\lambda_{min}(\mathbf{K})\|\mathbf{r}\|^2 \quad \leq \quad \mathbf{r}^T\mathbf{K}\mathbf{r} \leq \lambda_{max}(\mathbf{K})\|\mathbf{r}\|^2. \tag{5.13}$$

Taking into account Eq (5.13), the inequality is calculated as:

$$\int_0^{t_f} (\|\mathbf{r}\|)^{\mu}\, dt \leq \frac{\mathcal{L}(0)}{k_2\lambda_{min}(\mathbf{K})}\,,\ \forall t. \tag{5.14}$$

We now use Barbalat's lemma [30]. As a result, the proposed control system is stable. Moreover, the tracking error of the control system will converge to zero according to $\mathbf{r} \to 0$ with $t \to \infty$. Therefore, this means that the errors $\mathbf{e} \to 0$ and $\dot{\mathbf{e}} \to 0$ with $t \to \infty$. This analysis complements the contribution of this control proposal. In fact, it provides a stability analysis that includes the derivation of the adjustment rules for the adaptive component (AC).

6. Numerical simulation

This section presents numerical simulation results that demonstrate the viability of the proposed control technique. The simulations were performed using the MATLAB environment, based on the DDMR mobile robot model, taking into account dynamic uncertainties and external disturbances. Three simulations were carried out to evaluate the dynamic behavior of the robot under representative operating conditions. Simulation parameters used in the FO-STA control scheme are shown in Table 1.

Table 1. Gains and parameters used for the FO-STA-AC control scheme.

Parameters	Value
α	0.81
μ	0.5
λ_1	0.1
k_1	1.5
k_2	0.1

The first simulation evaluates the controller's capability to handle trajectories with discontinuities. The goal is to assess whether the control system can remain stable, avoid excessive deviations, and rapidly reestablish accurate tracking after abrupt directional transitions.

The second simulation studies the case of robot mass variation due to payload deliveries in motion or variation of the robot's center of mass due to payload displacement caused by acceleration.

The third simulation examines the controller's response to sudden parameter variations caused by a change in the robot's friction. The objective is to verify whether the controller can maintain accurate trajectory tracking despite abrupt dynamic disturbances.

For all cases, the controller-parameter estimators were initialized with estimated initial values to accelerate the convergence of the initial tracking error.

Furthermore, a subsection was added that compares the behavior of the proposal with other controllers in the literature.

6.1. Model uncertainty and non-linearities

In this simulation, the differential robot must follow two concentric trajectories using two different controllers: adaptive sliding mode control (SMC-AC) and the fractional-order-super-twisting algorithm proposed and developed in this work in conjunction with adaptive control. The robot has modeling uncertainties, both in some of its parameters (which are approximate) and in the model itself. In the case of the model, it is a linearized mathematical model, ignoring many nonlinear characteristics. Figure 3 of the first simulation shows the trajectories followed using both controllers, where a small radial difference can be seen. Figure 4 shows the torque control actions of the STA-AC strategy. Figure 5 shows the mean square error of both trajectories, and it can be seen that the FO-STA-AC strategy has a lower error than the traditional SMC. Figure 6 shows the reference generated by the kinematic control and the speed followed by the DDMR robot for FO-STA-AC control. With these results, it is easy to see that FO-STA-AC control has the ability to reduce errors due to model uncertainties. It is also worth noting that the controller is robust enough to follow the trajectory despite its discontinuities.

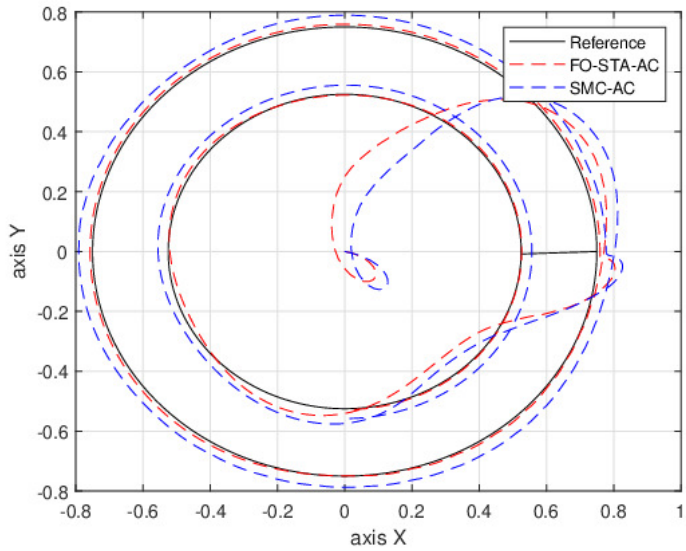

Figure 3. Trajectory tracking during the concentric circles trajectory simulation, highlighting the robot's behavior at discontinuities and the reestablishment of accurate tracking.

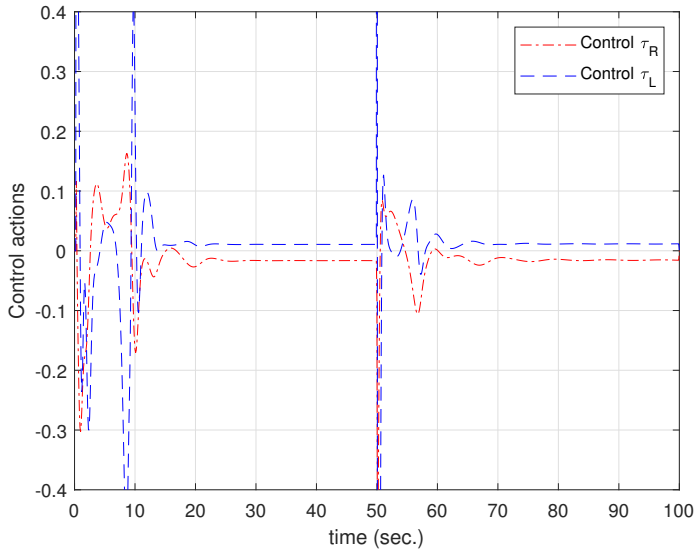

Figure 4. Control actions during the trajectory-discontinuity simulation, showing corrective responses at discontinuities.

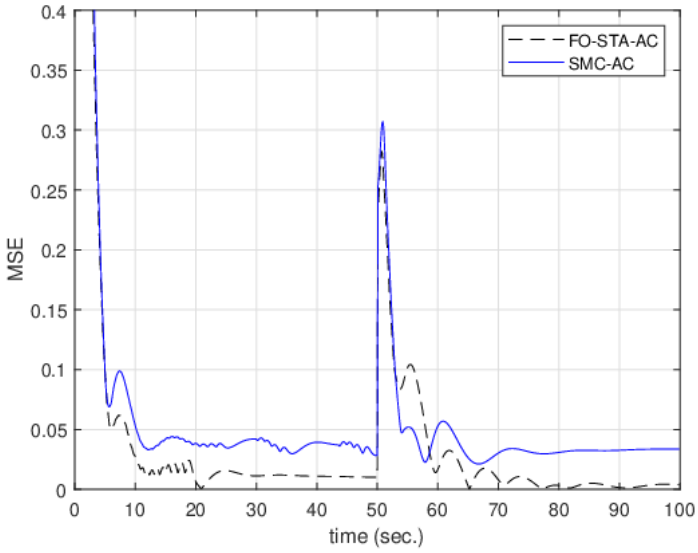

Figure 5. Mean squared tracking error (MSE) during the concentric circle simulation, including the transient deviations at each discontinuity.

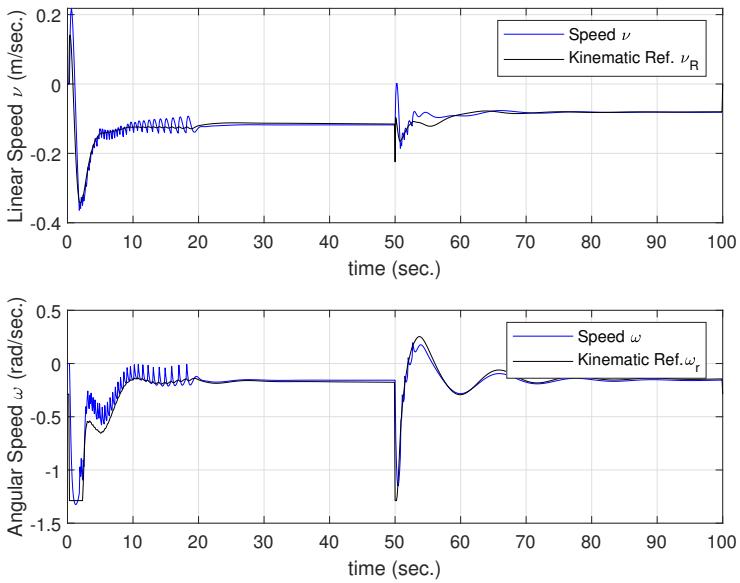

Figure 6. DDMR output speeds and references generated by kinematic control.

6.2. Parameter variations

This simulation studies the reaction of the FO-STA controller to payload variation when the robot is in motion. This situation may arise in the event that UAV vehicles deliver the payload to the DDMR while still following the pre-established trajectory. The simulation consists of simultaneously increasing the robot's mass (50 percent), inertia (50 percent), and friction coefficient (70 percent) due to the deformation of the pneumatic wheels. Figure 7 shows the circular trajectory; at first glance, the robot did not deviate from its trajectory. Figure 8 shows the control actions observing their reaction to parameter variations (50 sec.). Figure 9 shows the MSE of the trajectory error and the sudden increase in error at 50 sec. It can also be seen that the FO-STA-AC controller reduces the error, bringing it closer to the reference.

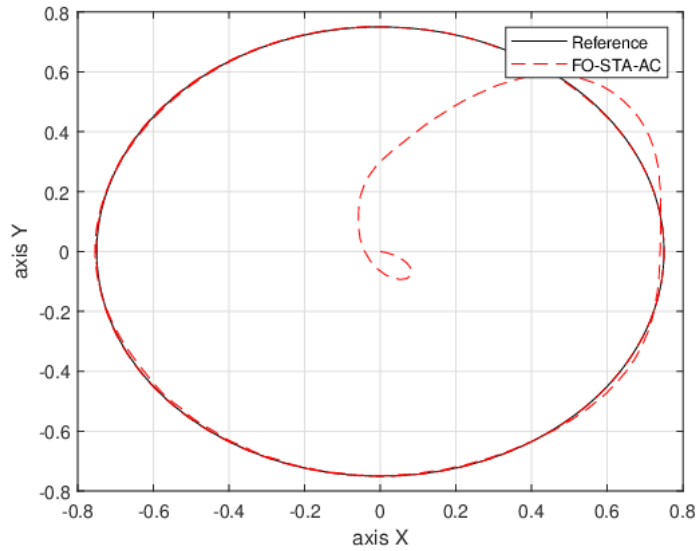

Figure 7. Trajectory tracking during the mass variation simulation.

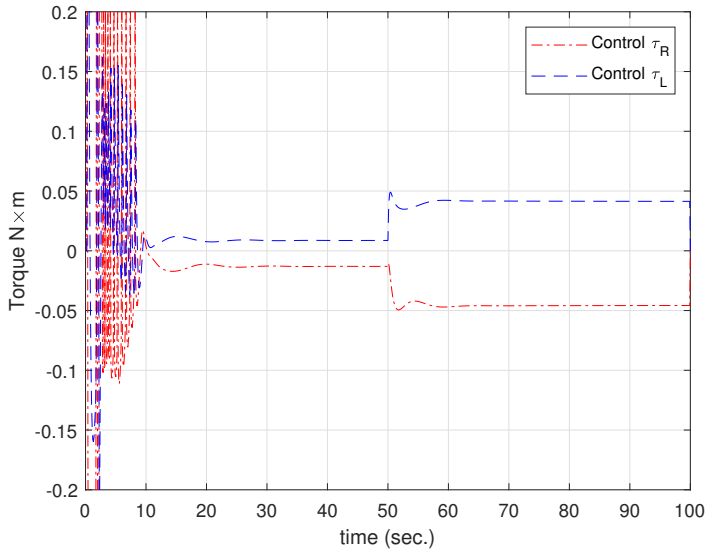

Figure 8. Control actions during the mass variations simulation, showing corrective responses at parameter variations.

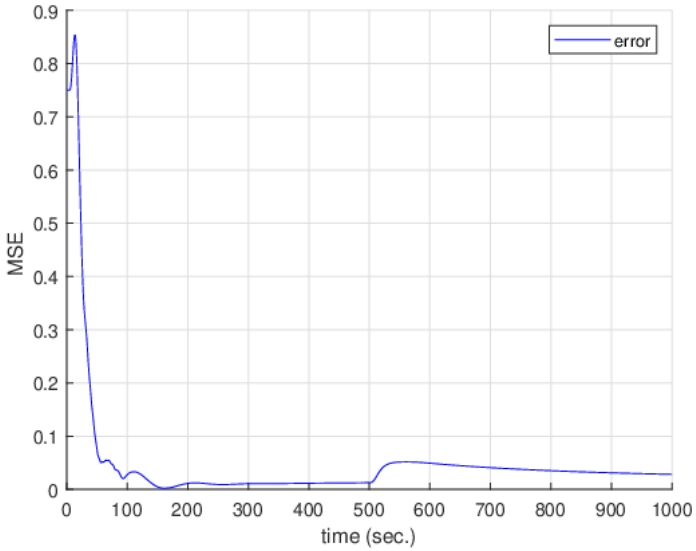

Figure 9. MSE error due to mass variations.

6.3. Comparative evaluation of sliding mode-based controllers

In the last simulation, variations in dynamics are produced to test the reaction capacity of the proposed control in the face of possible variations in the environment in a circular trajectory. In this case, the friction coefficient is increased by 70 percent at 60 seconds, simulating that the DDMR robot is moving on sand. It is easy to see in Figure 10 that the error increases, but the FO-STA-AC controller stabilizes the speed behavior by approximating the reference value generated by the kinematic control. In contrast, the SMC-AC control error is greater, even though the adaptive control attempts to make the correction. Figure 11 shows the trajectory followed using both controllers. It is clear that the error obtained is much smaller with the STA-AC control.

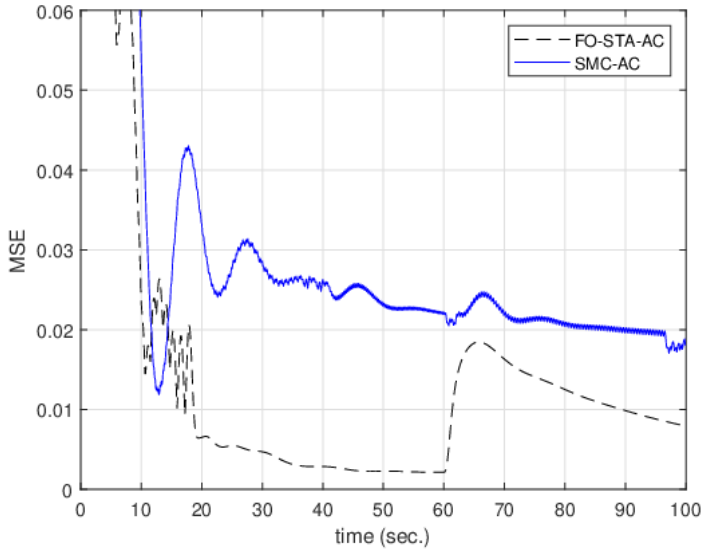

Figure 10. Tracking-error profiles obtained with the sliding-based controllers evaluated in MATLAB.

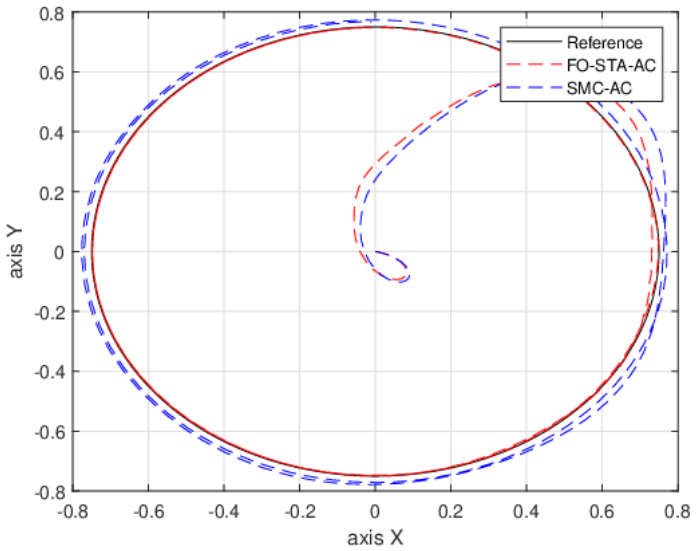

Figure 11. Trajectories followed by the mobile robot under each sliding mode-based controller (SMC and FO-STA).

6.4. Robustness tests

In previous simulations, the behavior of the control under dynamic variations (mass variation, friction, etc.) was studied. In this subsection, a robustness analysis will be implemented on the proposed controller. In this case, it will be the controller behavior for concentrated disturbance rejection. This will consist of applying a lumped disturbance that varies over time $\xi(t)$, simulating a possible combination of friction, wind, and uneven terrain. For this purpose, a sinusoidal disturbance

is used:

$$\xi(t) = a\sin(\omega t) + b, \tag{6.1}$$

where a and b are constants. The control action is disturbed with the signal $\xi(t)$ and the behavior of the controller is analyzed.

The simulation consisted of the DDMR robot following a circular trajectory while the disturbance $\xi(t)$ acted on the control action. Figure 12 shows the FO-STA controller action with the contaminated signal. Figure 13 indicates the speed references of the kinematic control and the robot speed output for the proposed control. In contrast, Figure 14 shows the trajectory followed by the robot with SMC and FOSTA control for the same disturbance. Finally, Figure 15 indicates the RMS error for both trajectories. It can be seen that FOSTA control has a smaller error than SMC control, which is due to the integral action of FOSTA. However, the settling time is similar.

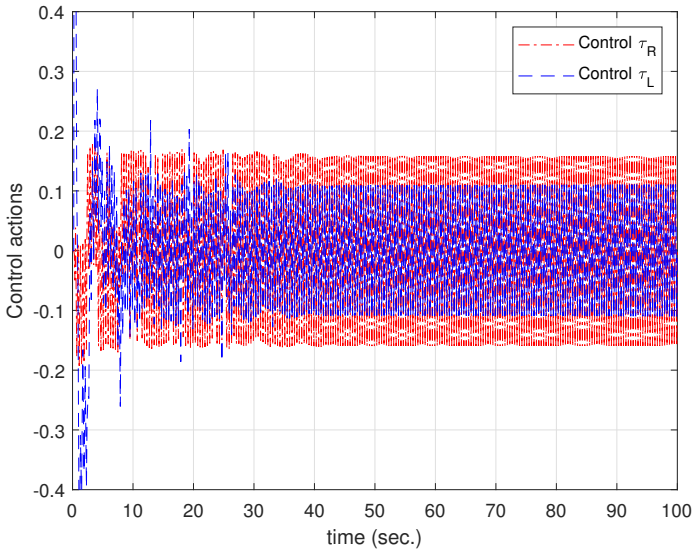

Figure 12. Control actions under external disturnace.

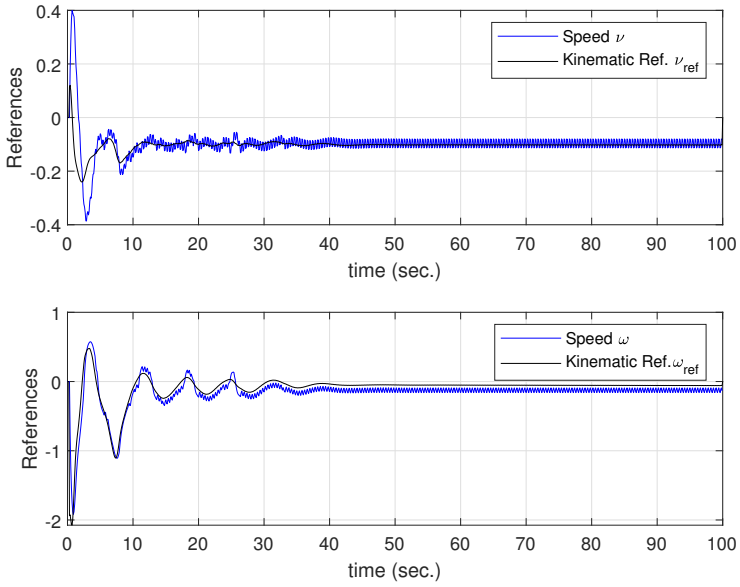

Figure 13. FOSTA reference and control action.

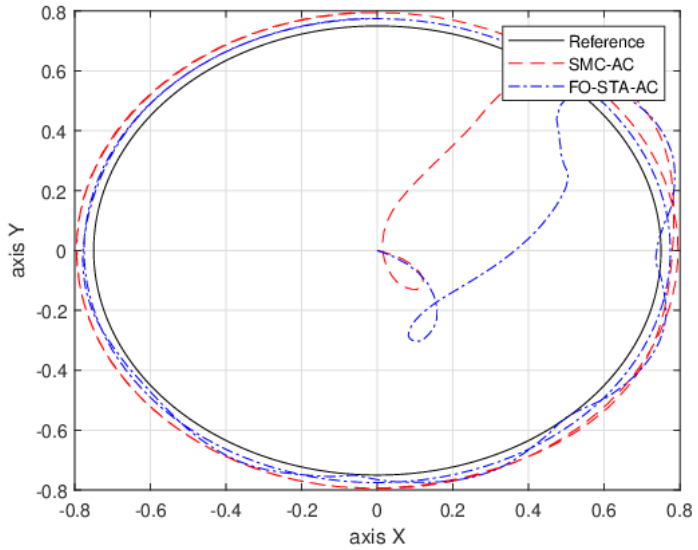

Figure 14. SMC and FOSTA controllers in trajectory tracking under external disturbances.

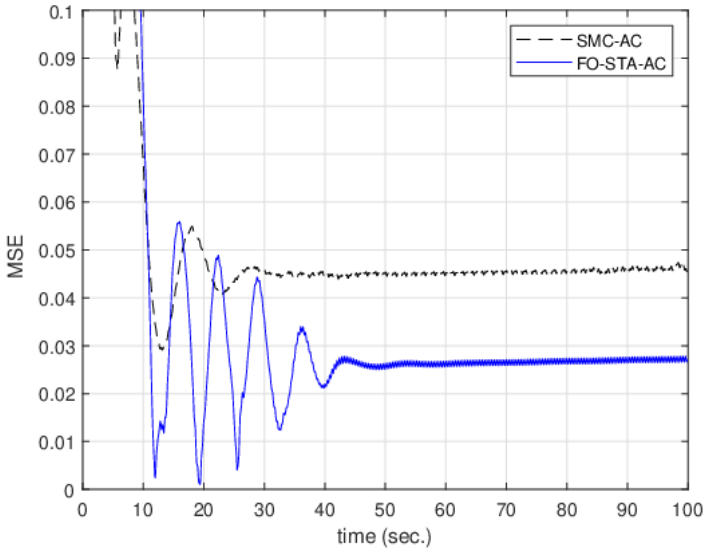

Figure 15. SMC (dashed line) and FOSTA (solid line) trajectory error.

In the second robustness test, noise is simulated in the speed sensors (v and ω) using additive white gaussian noise (AWGN) with a mean of zero and, in this case, a variance of $\sigma = 0.05$, which represent reasonable signal-to-noise ratio values. In the following, Figure 16 shows the control actions and Figure 17 shows the kinematic reference together with the speed output. Here, the variations produced by the effect of noise can be observed. Figure 18 shows the trajectory followed by the DDMR and, finally, the mean square error of the trajectory error is presented in Figure 19, which remains within reasonable tracking values.

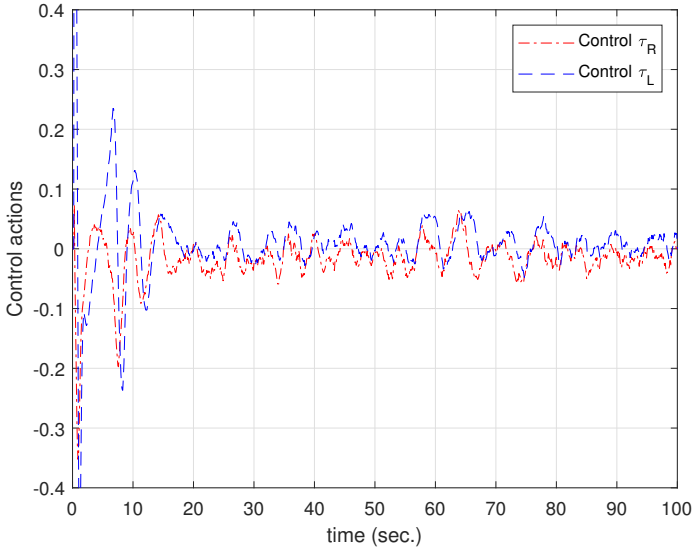

Figure 16. FOSTA control actions under AWGN.

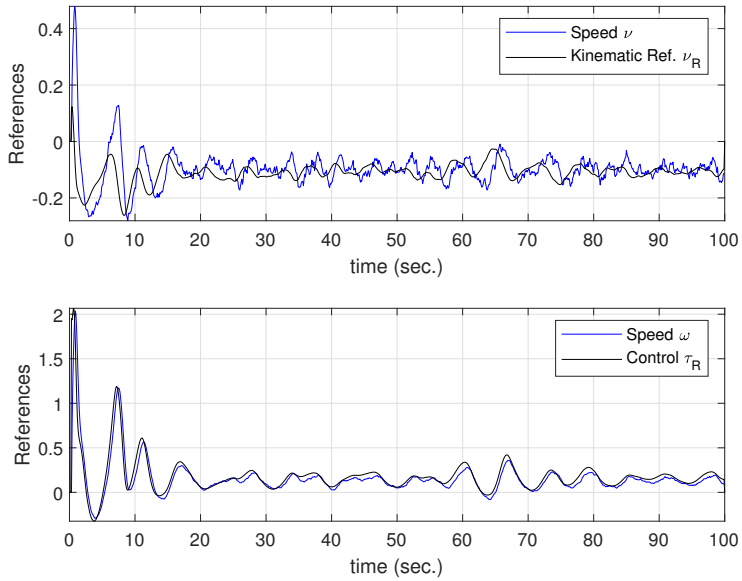

Figure 17. FOSTA references and output speeds.

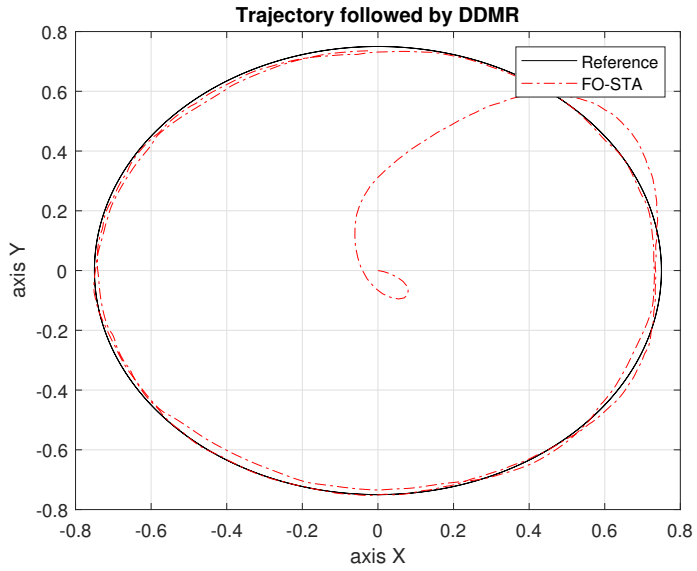

Figure 18. FOSTA trajectory under additive white gaussian noise (AWGN).

Figure 19. FOSTA trajectory error with AGWN.

7. Discussion

The simulation results collectively demonstrate the effectiveness and robustness of the proposed FO-STA-AC control strategy when applied to nonlinear DDMR dynamics subject to uncertainties, external disturbances, and nonsmooth reference trajectories. Both simulation scenarios highlight complementary aspects of controller behavior and allow for a broader interpretation of the framework's performance relative to classical SMC-based alternatives in DDMR applications.

In the first simulation, a sudden friction variation introduced a significant perturbation in the DDMR's dynamic parameters, emulating a representative situation in logistics and transport applications. The FO-STA-AC controller rapidly compensated for this variation and restored accurate trajectory tracking, confirming its capability to attenuate parametric disturbances that would otherwise degrade performance considering adaptive schemes. The transient increase in error followed by quick recovery illustrates the benefit of combining adaptive control with the FO-STA algorithm.

The second simulation evaluated the ability of the nested loop (kinematic-dynamic) control structure to handle nonsmooth reference trajectories. When tracking a concentric trajectories with abrupt directional transitions, the inverse-kinematics controller provided appropriate velocity references while the FO-STA-AC preserved dynamic stability, preventing divergence at each discontinuity. The short transients observed after circle change demonstrate the capacity of the overall structure to maintain performance under trajectory variations, which is a desiderable feature for mobile robots operating in constrained or cluttered environments. Robustness tests were also performed on the controller, using deterministic disturbances and white noise in the sensors, which demonstrated good disturbance rejection capabilities.

These observations reinforce the relevance of incorporating adaptive control in FO-STA architectures for mobile robot applications.

Taken together, the simulations confirm that the FO-STA-AC architecture provides a flexible, robust, and effective framework for dynamic compensation in DDMR operating under uncertain and varying

conditions. Its performance advantages emerge more clearly when contrasted with simpler sliding-based formulations, suggesting that the integration of adaptive approximators plays a central role in achieving reliable tracking in realistic dynamic scenarios.

8. Conclusions

This paper presents a control technique for a DDMR for trajectory tracking, taking into account its dynamic variations and unmodeled dynamics. To achieve this, nonlinear control techniques were used, including stability analysis, from which the control law adjustment rules were obtained. The proposed DDMR control uses two nested loop controllers, a kinematic control for the external control loop and a dynamic control (FO-STA-AC) for the internal loop, the latter being the most complex and responsible for compensating for the uncertainties in the model. The dynamic proposal (FO-STA-AC) takes into account two key characteristics for its development: the robustness of second-order sliding mode control, together with the dynamic updating of controller parameters using an adaptive technique. This synergy between the two techniques helps to reduce control errors in trajectory tracking. The proposal guarantees the asymptotic stability of the closed-loop system, taking into account external disturbances and dynamic uncertainties. In addition to the Lyapunov analysis demonstrating the stability of the proposed technique, this is also reflected in the simulations. These numerically and analytically demonstrate that the FO-STA-AC combination produces excellent results. Furthermore, They do not require adjusting the FO-STA gains (k_1, k_2), as the adjustment is made through the estimated parameters of the robot. Therefore, the proposed control approach is an effective solution to the trajectory tracking problem in DDMRs considering their dynamics. Future work will focus on systems with more complex dynamics (SSMR, omnidirectional, UAV) to evaluate the behavior of this type of strategy.

Author contributions

Conceptualization, F. R. S. B., F. S. A, S. K., F. C, and J. U.; Data curation, S. K. and J. U.; Formal analysis, S. B. and F. B. Funding acquisition, S. B.; Investigation, S. B., F. S. A., F. B., F. C., and J. U.; Methodology, F. R.; Project administration, S. B.; Resources, S. B. and S. K.; Software, J. U.; Supervision, S. B. and F. R.; Validation, S. B., E. Z., F. C., and F. S. A. Writing—original draft, F. R. and F. C; Writing—review and editing, F. S. A. and F. B.

Use of Generative-AI tools declaration

The authors declare they have not used Generative Artificial Intelligence (AI) tools in the creation of this article.

Acknowledgments

This work was funded by the University of Jeddah, Jeddah, Saudi Arabia, under grant N°. (UJ-24-DR-20772-1). Therefore, the authors thank the University of Jeddah for its technical and financial support.

Conflict of interest

All authors declare no conflicts of interest in this paper.

References

1. H. Wang, Y. Huang, Y. Ge, W. Gao, Trajectory tracking control for mobile robots based on second order fast terminal sliding mode, In: *2018 33rd Youth Academic Annual Conference of Chinese Association of Automation (YAC)*, 2018, 581–584. https://doi.org/10.1109/YAC.2018.8406441
2. V. Nguyen, M. T. Vu, S. H. Kim, A finite-time non-singular fast terminal sliding mode control of wheeled mobile robots with prescribed performance, *IET Control Theory A.*, **19** (2025), e70013. https://doi.org/10.1049/cth2.70013
3. H. Ríos, M. Mera, A. Polyakov, Perturbed unicycle mobile robots: A second-order sliding-mode trajectory tracking control, *IEEE T. Ind. Electron.*, **71** (2024), 2864–2872. https://doi.org/10.1109/TIE.2023.3270520
4. G. J. E. Scaglia, M. E. Serrano, S. A. Godoy, F. Rossomando, Linear algebra-based controller for trajectory tracking in mobile robots with additive uncertainties estimation, *IMA J. Math. Control I.*, **37** (2020), 607–624. https://doi.org/10.1093/imamci/dnz016
5. Z. Sun, H. Xie, J. Zheng, Z. Man, D. He, Path-following control of mecanum-wheels omnidirectional mobile robots using nonsingular terminal sliding mode, *Mech. Syst. Signal Pr.*, **147** (2021), 107128. https://doi.org/10.1016/j.ymssp.2020.107128
6. A. H. Nezhad, M. R. Soltanpour, S. Zaare, Observer-based robust finite-time tracking control for two-wheeled balancing mobile robots in the presence of uncertainties, *Robot. Auton. Syst.*, **202** (2026), 105456. https://doi.org/10.1016/j.robot.2026.105456
7. S. Yin, C. Chen, Z. Xiang, Distributed predefined-time leader-follower formation control for heterogeneous wheeled mobile robots, *IEEE T. Autom. Sci. Eng.*, **23** (2026), 6687–6697. https://doi.org/10.1109/TASE.2026.3673594
8. J. Uliarte, E. O. Freire, F. U. Vázquez, F. Camargo, H. Secchi, R. Carelli, et al., Trajectory tracking of a wmr using a neuro-adaptive mrac control with dynamic uncertainties, *IEEE Access*, **14** (2026), 37871–37884. https://doi.org/10.1109/ACCESS.2026.3670760
9. S. Boubaker, J. Gaia, E. Zavalla, S. Kamel, F. S. Alsubaei, Fa. Bourennani, et al., Trajectory tracking of wmr with neural adaptive correction, *Mathematics*, **13** (2025), 3178.https://doi.org/10.3390/math13193178
10. L. Caracciolo, A. de Luca, S. Iannitti, Trajectory tracking for a four-wheel differentially driven mobile robot, In: *Proceedings 1999 IEEE International Conference on Robotics and Automation*, **4** (1999), 2632–2638. https://doi.org/10.1109/ROBOT.1999.773994
11. J. Moreno, E. Slawiñski, F. A. Chicaiza, F. G. Rossomando, V. Mut, M. A. Morán, Design and analysis of an input–output linearization-based trajectory tracking controller for skid-steering mobile robots, *Machines*, **11** (2023), 988. https://doi.org/10.3390/machines11110988

12. C Canudas de Wit, H. Khennouf, C. Samson, O. J. Sordalen, Nonlinear control design for mobile robots, In: *Recent trends in mobile robots*, 1993, 121–156. https://doi.org/10.1142/9789814354301_0005

13. H. Xie, J. Zheng, Z. Sun, H. Wang, R. Chai, Finite-time tracking control for nonholonomic wheeled mobile robot using adaptive fast nonsingular terminal sliding mode, *Nonlinear Dyn.*, **110** (2022), 1437–1453. https://doi.org/10.1007/s11071-022-07682-2

14. T. N. T. Cao, B. T. Pham, N. T. Nguyen, D. Vu, N. Truong, Second-order terminal sliding mode control for trajectory tracking of a differential drive robot, *Mathematics*, **12** (2024), 2657, 2024.https://doi.org/10.3390/math12172657

15. Y. Liu, G. Cui, Z. Li, Fixed-time consensus control of stochastic nonlinear multi-agent systems with input saturation using command-filtered backstepping, *AIMS Math.*, **9** (2024), 1476514785. https://doi.org/10.3934/math.2024718

16. J. Zhai, Z. Song, Adaptive sliding mode trajectory tracking control for wheeled mobile robots, *Int. J. Control*, **92** (2019), 2255–2262. https://doi.org/10.1080/00207179.2018.1436194

17. S. Ahmed, A. T. Azar, I. K. Ibraheem, Model-free scheme using time delay estimation with fixed-time fsmc for the nonlinear robot dynamics, *AIMS Math.*, **9** (2024), 9989–10009. https://doi.org/10.3934/math.2024489

18. A. Mallem, S. Nourredine, W. Benaziza, Mobile robot trajectory tracking using pid fast terminal sliding mode inverse dynamic control, In: *2016 4th International Conference on Control Engineering & Information Technology (CEIT)*, 2016, 1–6. https://doi.org/10.1109/CEIT.2016.7929057

19. I. Salgado, D. Cruz-Ortiz, O. Camacho, I. Chairez, Output feedback control of a skid-steered mobile robot based on the super-twisting algorithm, *Control Eng. Pract.*, **58** (2017), 193–203. https://doi.org/10.1016/j.conengprac.2016.10.003

20. Y. B. Shtessel, J. A. Moreno, F. Plestan, L. M. Fridman, A. S. Poznyak, Super-twisting adaptive sliding mode control: A lyapunov design, In: *49th IEEE Conference on Decision and Control (CDC)*, 2010, 5109–5113. https://doi.org/10.1109/CDC.2010.5717908

21. A. Tattersall, B. McGuinness, H. Lim, C. K. Au, H. Williams, M. Duke, The effect of dimensional parameters on the performance of ddmrs, In: *2023 IEEE 19th International Conference on Automation Science and Engineering (CASE)*, 2023, 1–6. https://doi.org/10.1109/CASE56687.2023.10260635

22. Y. Chen, I. Petras, D. Xue, Fractional order control-a tutorial, In: *2009 American control conference*, 2009, 1397–1411. https://doi.org/10.1109/ACC.2009.5160719

23. J. E. Macías-Díaz, Fractional calculus—theory and applications, **11** (2022), 43. https://doi.org/10.3390/axioms11020043

24. Z. Li, L. Liu, S. Dehghan, Y. Chen, D. Xue, A review and evaluation of numerical tools for fractional calculus and fractional order controls, *Int. J. Control*, **90** (2017), 1165–1181. https://doi.org/10.1080/00207179.2015.1124290

25. A. P. Singh, K. Bingi, Applications of fractional-order calculus in robotics, *Fractal Fract.*, **8** (2024), 403. https://doi.org/10.3390/fractalfract8070403

26. V. Mihaly, M. Şuşcă, D. Morar, M. Stănese, P. Dobra, μ-Synthesis for fractional-order robust controllers, *Mathematics*, **9** (2021), 911. https://doi.org/10.3390/math9080911

27. I. Matraji, K. Al-Wahedi, A. Al-Durra, Higher-order super-twisting control for trajectory tracking control of skid-steered mobile robot, *IEEE Access*, **8** (2020), 124712–124721. https://doi.org/10.1109/ACCESS.2020.3007784

28. I. Matraji, A. Al-Durra, A. Haryono, K. Al-Wahedi, M. Abou-Khousa, Trajectory tracking control of skid-steered mobile robot based on adaptive second order sliding mode control, *Control Eng. Pract.*, **72** (2018), 167–176. https://doi.org/10.1016/j.conengprac.2017.11.009

29. C. Rosales, C. V. Sisterna, F. Rossomando, D. Gandolfo, C. Soria, R. Carelli, Super-twisting adaptive control of a quadrotor, *ISA T.*, **166** (2025), 241–249. https://doi.org/10.1016/j.isatra.2025.07.029

30. J. J. E. Slotine, W. Li, *Applied nonlinear control*, Prentice Hall, 1991.

Appendix

A. Appendix 1

This section presents the values of the parameters of the DDMR robot used in the simulation (Table 2).

Table 2. DDMR simulation parameters.

Parameter	Value
r	0.095 m
L	0.330 m (approx.)
m	9 kg.
J_z	0.35 kg×m^2
I_w	0.001 kg×m^2
a_0	0.10 m (approx.)